A Computational Fluid Dynamics Investigation Comparing the Performance of an Alternative Valvetrain Design Against a Traditional Poppet Valvetrain

Austin Clay Robinson
Department of Mechanical Engineering,
University of North Carolina at Charlotte,
Charlotte, NC 28223
e-mail: arobi100@uncc.edu

Norman H. Garrett
Department of Mechanical Engineering,
University of North Carolina at Charlotte,
Charlotte, NC 28223
e-mail: ngarret6@uncc.edu

Darrick Vaseleniuck
Vaztec, LLC.,
Mooresville, NC 28115
e-mail: darrickv@vaztec.com

Mesbah Uddin
Department of Mechanical Engineering,
University of North Carolina at Charlotte,
Charlotte, NC 28223
e-mails: mesbah.uddin@uncc.edu;
muddin@uncc.edu

The poppet valve is by far the most widely used in cylinder head design of internal combustion (IC) engines; however, poppet valves themselves create significant flow restrictions during both the intake and exhaust strokes, thus causing a reduction in volumetric efficiency that affects overall engine performance. By removing the restrictive poppet valve from the flow path of air into and out of the cylinder head and allowing air to flow unobstructed, any given IC engine can achieve greater volumetric efficiency and higher specific output. The Vaztec ECOREV rotary valve system utilizes straight-cut flow passages that reduce such restrictions. This rotary valve system is designed to be directly driven by the crankshaft, thereby replacing the camshaft and poppet valve system altogether. This paper will primarily explore the differences in flow characteristics between this rotary valve and a conventional poppet valve cylinder head using both computational fluid dynamics (CFD) and flow bench data. Both configurations will be evaluated on the same single-cylinder four-stroke internal combustion engine. CFD simulations were run at multiple valve opening positions on each cylinder head configuration for both intake and exhaust cycles to validate the CFD process against flow bench test data for both cylinder head designs. The CFD was performed in 3D using hexahedral meshing and steady-state Reynolds-averaged Navier–Stokes (RANS) turbulence models. Comparison between the two engine configurations will include both intake and exhaust airflow rates as well as discharge coefficients and overall flow field evaluation using numerous scalar and vector properties.
[DOI: 10.1115/1.4054966]

Keywords: aerodynamics, CFD-methods, computational fluid dynamics, engines

1 Introduction

Modern internal combustion (IC) engines are becoming increasingly more complex due to growing international scrutiny on emissions and efficiency targets. The result is that engine development gains are expensive and incremental. Electric vehicles are quickly beginning to take hold in the marketplace, and in this environment, new technological breakthroughs are required to keep IC engines relevant. At its most basic level, a combustion engine requires efficient delivery of air and fuel in order to achieve combustion. In comparison to increasing air flow in an existing engine design, fuel flow is relatively simple to add, with the addition of larger jets (in the case of a carbureted engine) or higher-powered pumps and larger injectors (for fuel injected systems). Air induction, however, is much more complicated to improve. Much focus has been placed on air induction improvements over the last several decades, from variable valve timing to turbochargers and superchargers. Poppet valve designs, however, have remained relatively unchanged apart from slight changes to geometry and materials. The fundamental challenge remains that the poppet valve is an inherently inefficient aerodynamic design with a relatively low discharge coefficient.

There have been many attempts at rotary valvetrain designs intended to replace the poppet valve with a solution that has a higher discharge coefficient [1–4]. In interest of brevity, these other rotary valve designs will not be visited in detail, but please see the references for more information. None of these designs have found widespread adoption. While the rotary valve designs mentioned all differ, they are based on the same principle: creating a valve with as a high discharge coefficient (C_D) as possible to maximize airflow into and out of the combustion chamber. Efficient gas transfer increases volumetric efficiency of an engine which can lead to increased specific output and better fuel economy. Beyond gas exchange properties, rotary valves can offer mechanical, thermal, and other advantages over a traditional poppet valvetrain, but this paper will focus solely on the flow characteristics.

Generally, issues with high-pressure sealing and the high wear-rates in rotary valve designs have prevented them from achieving commercial success [4]. Previous designs have used high seal-to-valve pressures as a method to achieve viable sealing. This, however, led to high friction and wear-rates. Some historical designs used lubrication to offset the wear and friction issues, but this led to high oil consumption and poor hydrocarbon emissions. The design under consideration in this paper addresses these sealing and friction issues with a combination of material selections and dynamic seal design [5]. The design presented in this paper has undergone hundreds of hours of actual engine dynamometer testing in multiple configurations and exhibited no sealing or undue friction issues. These topics, however, will be covered in a future paper.

Referring to Fig. 1, showing a cross-sectional view of a dual rotary valve cylinder head, it can be seen that a rotary valve can provide an unobstructed flow path into and out of the combustion chamber. This contrasts with a poppet valve system which always has an obstructive valve head constricting the gas exchange processes.

Manuscript received March 22, 2022; final manuscript received July 7, 2022; published online August 2, 2022. Assoc. Editor: Bengt Sunden.

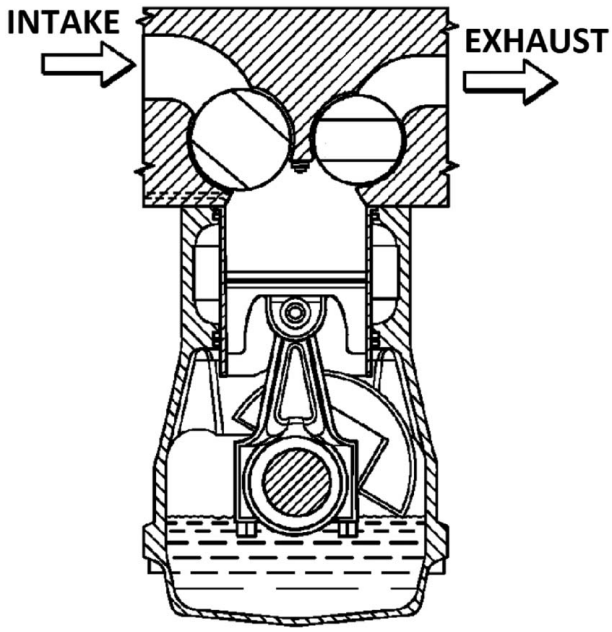

Fig. 1 A dual rotary valve cylinder head

There are a variety of methods of determining the flow characteristics of a cylinder head [6], but this paper will focus on two: flow bench testing and computational fluid dynamics (CFD). A flow bench is a common real-world test designed to measure the volumetric flow rate of air through an intake or exhaust port at a given pressure. This method can be valuable for cylinder head tuning, but the data available are somewhat limited beyond the volumetric flow rate. However, these data can be used to determine the discharge coefficient of a given flow orifice. CFD enables measurement not only of the flow rate but also a vast array of other flow properties. For this reason, the research performed for this paper involved both flow bench and CFD testing to capture as much data as possible regarding the flow field through the poppet and rotary valve cylinder heads to better understand the differences between the two designs. The data collected allowed for a comparison of the C_D of both cylinder head designs as well as the underlying flow characteristics of each design.

Both the experimental and CFD testing were conducted in the Motorsports Research Center at The University of North Carolina at Charlotte.

2 Theory

The discharge coefficient is a ratio of actual to theoretical mass flow through an orifice [7].

$$C_D = \frac{\dot{m}_{\text{act}}}{\dot{m}_{\text{th}}} \tag{1}$$

The actual mass flow rate ($\dot{m}_{\text{act}}$) is measured experimentally, and the theoretical mass flow rate ($\dot{m}_{\text{th}}$) is determined through isentropic analysis of the physical flow conditions. Ambient air density and pressure are denoted by ρ_a and p_a, respectively.

$$\dot{m}_{\text{th}} = A_{\text{ref}} \sqrt{\rho_a p_a} * \varphi \tag{2}$$

$$\varphi = \sqrt{\frac{2k}{k-1}\left(\left(\frac{p_a}{p_t}\right)^{2/k} - \left(\frac{p_a}{p_t}\right)^{(k+1)/k}\right)} \tag{3}$$

The symbol φ represents the isentropic flow coefficient [8]. p_t is the test pressure and k is the specific heat ratio of air. The reference area (A_{ref}) is the effective flow area of the valve. For the poppet valve, this area is the valve curtain area (A_c), calculated using the valve lift (L_v) and valve head diameter (D_v). For the rotary valve, the reference area is simply the area of the valve port.

$$A_{\text{ref}} = A_c = \pi D_v L_v \tag{4}$$

In addition to the discharge coefficient, volumetric efficiency (η_v) is another common index used to benchmark the air induction system [9]. V_d is the displacement volume of the engine, N is revolutions per minute, and $\dot{m}_a$ is the mass flow rate of air through the engine.

$$\eta_v = \frac{\dot{m}_a}{\rho_a V_d N} \tag{5}$$

Equation (5) shows the direct proportionality between the mass flow of air and the volumetric efficiency of a system. The research performed for this paper assumed steady-state operation. Dynamic flow considerations are beyond the scope of this paper. However, due to the direct correlation between mass flow and η_v, performance comparisons can be extrapolated.

3 Rotary Valve Design

The basis for the rotary valve cylinder head design was a commercially available 435 cc (26.5 in.^{3}) single-cylinder overhead valve (OHV) engine. The selection of a single-cylinder, two-valve engine as the base was to allow for the simplest possible comparison between the rotary and poppet valve heads. The dual rotary valves modeled in this paper (see Fig. 1) are each cylindrical and on parallel axes of rotation with the crankshaft. The valves are directly driven by the crankshaft at a 4:1 ratio of crankshaft to valve rotation speed. This ratio is achieved by virtue of the symmetrical valves, which are fully open twice per valve rotation. The cylinder head itself is a two-piece design, with the valves fitted between the upper and lower head pieces. These upper and lower components perform the sealing function between the valve and the cylinder head.

Figures 2 and 3 show cutaway views of a single-shaft rotary valve engine during the intake and exhaust strokes, respectively.

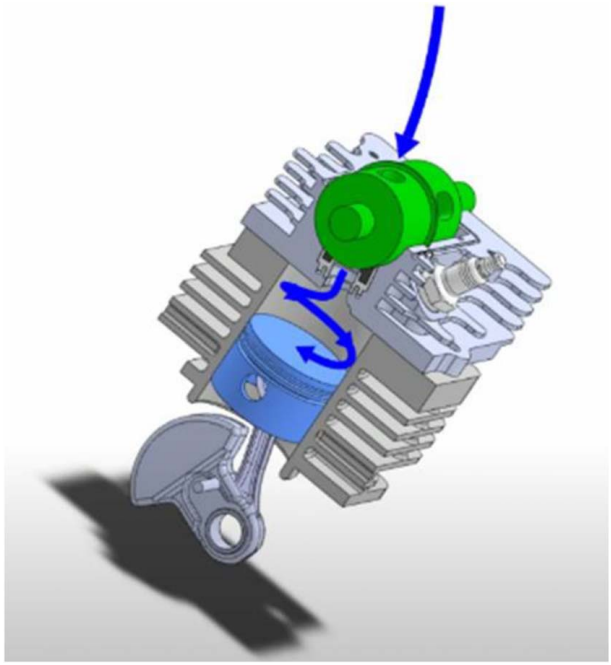

Fig. 2 Single rotary valve engine: intake stroke

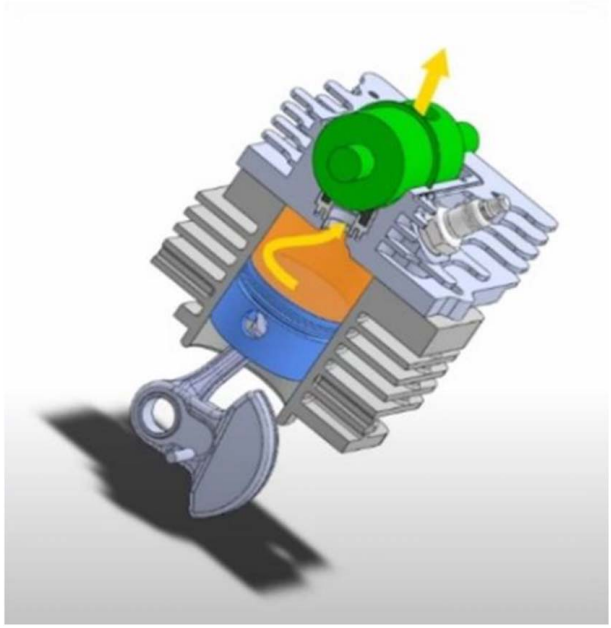

Fig. 3 Single rotary valve engine: exhaust stroke

This single-shaft system is shown for illustrative purposes—the flow paths apply to both single and dual-shaft valve systems.

The rotary valve ports were sized to match the minimum throat areas of the corresponding intake and exhaust ports of the poppet valve cylinder head. This sizing was chosen to create a valid comparison between the two cylinder head designs. Matching the minimum port area for the intake and exhaust sections of the stock cylinder head resulted in the rotary valves themselves having an area deficit with respect to the flow areas of the respective poppet valves (see Table 1). The poppet intake valve curtain area is 37% larger than the rotary inlet valve of this study. The poppet exhaust valve curtain area is 69% larger than the flow area of the rotary exhaust valve port area. This disparity will be discussed more later in this paper. Valve duration was designed to be consistent between the poppet and rotary valve engines. Table 1 shows the valve dimensions of both systems. The poppet valve curtain areas are larger than the rotary valve port areas for both intake and exhaust.

4 Experimental Setup

The physical steady-state flow testing was conducted using a Superflow SF-600 flow bench. Figure 4 shows the flow bench with the poppet valve cylinder head attached for testing. The flow bench was calibrated to manufacturer specifications before the testing was conducted on the different cylinder heads. Ambient temperature for all flow bench testing was held at 71 °F (22 °C). A flow bench cylinder size of 3.5 in. (88.9 mm) was chosen, as the closest available size to the engine bore size of 3.386 in. (86 mm). The bore size discrepancy of 0.114 in. (2.9 mm) was assumed to be small enough as to have a negligible effect on flow performance. For each test, the pressure differential between atmospheric conditions and the test plenum within the flow bench was set to 25 in. of water (6.221 kPa). Each cylinder head (rotary valve or poppet valve) was tested in both the intake and exhaust configuration, with flow direction set appropriately. Each configuration was tested at eight increments from closed to fully open. As the conventions for valve opening differ between a poppet valve (lift) and a rotary valve (rotational angle), both were converted to a "percent duration" value for direct comparison, as shown in Table 2. Since flow performance is assumed to be symmetrical, data from 0% to 50% were mirrored in the analysis.

The flow bench data collected using these positional increments will be shown in the results section. The flow measurements on the SF-600 are taken with an inclined analog manometer, with a published accuracy within ±2.5%. Measurements were taken in cubic feet per minute (CFM) of air flow.

5 Computational Fluid Dynamics Study

Four separate computer aided design (CAD) models were used in the simulation, incorporating an intake and exhaust version of each cylinder head. For simplification, each model contained only the pertinent intake or exhaust valve/port. For each configuration, the opposing unused (closed) valve was removed from the model and the spark plug holes were eliminated to simplify the computation for the CFD software and reduce simulation times. It was assumed that these modifications had no significant impact on either the mass flow rate through the ports or the overall flow fields. These CAD models are shown in Figs. 5–8.

All CFD simulations were performed using a steady-state Reynolds-averaged Navier–Stokes, realizable k–ε turbulence model (RKE) with all-y+ wall treatment [10]. This model was selected after comparing the results of simulations using several turbulence models, shown in Table 3. The other models used were shear stress transport (SST) k–ω, Abe–Kondoh–Nagano k–ε (AKN), elliptic blending k–ε (EB), and V2F k–ε (V2F) [11–14]. RKE was selected as it performed closest to the experimental flow rate values over the range of cases. In most cases, the other four turbulence models underpredicted the flow rate by a larger margin that did the RKE model. Additionally, the V2F model caused stability issues with the exhaust simulations, which is why the values are listed as N/A—the simulations did not converge to a final value. While all five models performed somewhat similarly in the rotary valve exhaust case, the performance over all cases of the RKE model led to its selection.

5.1 Meshing. To make the necessary geometric simplifications and to remove any imperfections in the surface detail from the CAD software, the models were brought into the ANSA software package for cleaning and surface meshing. Once the surface meshing was complete, the models were brought into STARCCM+ for the remainder of the process, including surface re-meshing, volume meshing, CFD simulation, and post-processing. Each model was meshed using the same trimmed-cell hexahedral mesh. Additionally, a prism layer mesher was used on the critical flow areas to accurately capture the boundary layer and any near wall effects on the flow. Prism layers were only used on the valves and ports in order to reduce the cell count for more efficient computation.

Volume meshing is a key step in the CFD process, as mesh size can directly influence the flow solver. Too coarse a mesh can lead to computational errors, and too fine a mesh can reduce the

Table 1 Valve area comparison

Poppet intake valve sizing	Poppet valve curtain area	Rotary valve opening area
Intake valve area (1.414 in. diameter poppet valve at max lift (0.400 in.), rotary at fully open)	1.777 in.^{2} (45.14 mm^2)	1.296 in.^{2} (32.92 mm^2)
Exhaust valve area (1.141 in. diameter poppet valve at max lift (0.400 in.), rotary at fully open)	1.435 in.^{2} (36.45 mm^2)	0.847 in.^{2} (21.51 mm^2)

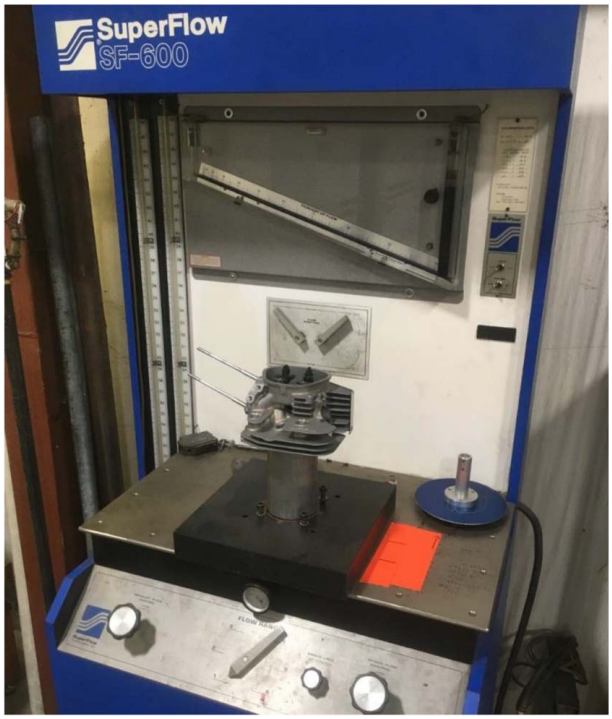

Fig. 4 SF-600 flow bench with poppet valve cylinder head

Table 2 Valve opening convention

% Duration	Poppet valve lift (in.)	Rotary valve angle (deg)
6.25	0.050	5.0
12.50	0.100	10.0
18.75	0.150	15.0
25.00	0.200	20.0
31.25	0.250	25.0
37.50	0.300	30.0
43.75	0.350	35.0
50.00	0.400	40.0

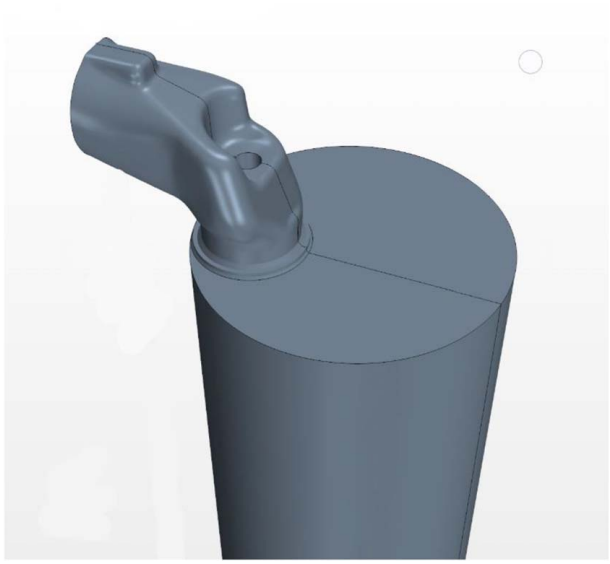

Fig. 5 CAD geometry, poppet valve cylinder head in exhaust configuration

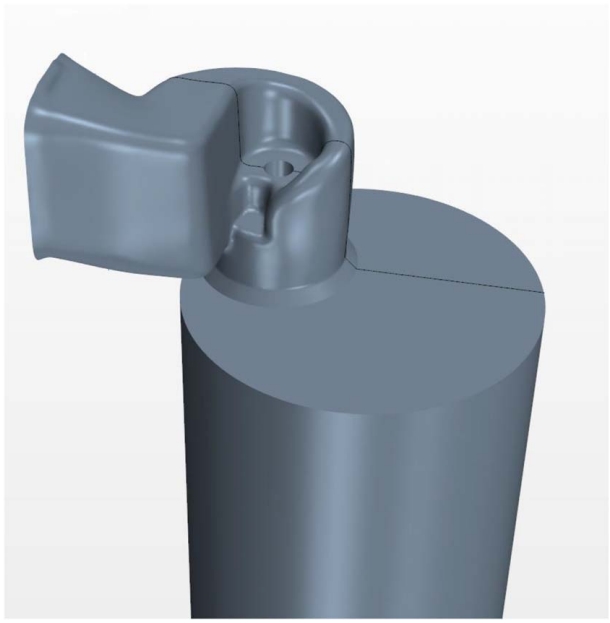

Fig. 6 CAD geometry, poppet valve cylinder head in intake configuration

computational efficiency. Consequently, mesh size selection was an iterative process. Starting with a coarse mesh, the cell size was reduced until the incremental change in mesh size no longer had a significant effect on the outcome of the simulation. All mesh refinement steps were performed on each model used in order to verify that the appropriate mesh size was used. After mesh convergence was reached, the final mesh settings, as seen in Fig. 9, were selected. The plane sections shown in Fig. 9 are at the symmetry plane of each valve, denoted by the black lines in Figs. 5–8. The base cell size of 0.5 mm was used in the flow ports, as this region was the most important. Cell size was expanded from there using volumetric meshing controls. Figure 9 also shows the virtual

Fig. 7 CAD geometry, rotary valve cylinder head in exhaust configuration

Fig. 8 CAD geometry, rotary valve cylinder head in intake configuration

Table 3 CFD turbulence model comparison

	Rotary valve		Poppet valve	
Method	Inlet CFM	Outlet CFM	Inlet CFM	Outlet CFM
Flow bench experiment	164.4	107.4	95.4	77.4
RKE	163.78	102.24	96.1	76.67
SST	159.96	99.31	90.96	70.89
AKN	156.50	102.52	90.63	69.40
EB	158.31	101.65	92.57	71.66
V2F	159.35	N/A	92	N/A

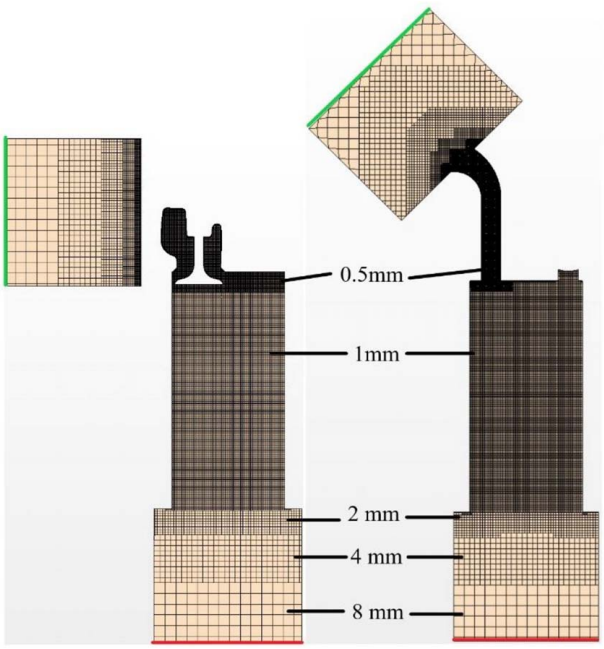

Fig. 9 Mesh diagram. Mesh of the rotary and poppet valves in their intake configuration is shown here.

Table 4 Mesh independence table: rotary valve

Exhaust		Intake	
Cell count (millions)	Plane CFM	Cell count (millions)	Plane CFM
1.30	102.21	0.57	184.52
1.80	102.40	1.06	183.46
2.75	102.04	2.08	183.24
3.71	101.91	2.56	184.05
6.30	102.24	*5.55*	171.87
7.71	101.85	10.32	170.46

Table 5 Mesh independence table: poppet valve

Exhaust		Intake	
Cell count (millions)	Plane CFM	Cell count (millions)	Plane CFM
0.94	77.44	0.76	99.73
1.26	78.56	1.06	99.26
1.97	78.67	1.60	93.97
3.00	77.19	3.01	96.04
5.25	76.67	*4.95*	96.10

plenums that were created. The purpose of these plenums was to stabilize the flow solver and allow for development of the flow field.

The final base size of the mesh was determined using an iterative process, starting with a coarse mesh size and refining until the change in mesh size no longer significantly affected the value of the mass flow rate. Tables 4 and 5 show the final cell counts of the mesh refinement steps and the corresponding flow rates in CFM. These results are for the wide-open intake and exhaust ports. These tables show that there was no discernable correlation between mesh size and the outcomes of the simulations. The rotary valve intake configuration shown on the right side of Table 4 was the simulation that ultimately led to the selection of the 0.5 mm base cell size. There was a large drop in the flow rate between 2.56 and 5.55 million cells.

Because of the large drop-off, a finer simulation with mesh of 10.32 million cells was run, but that showed no significant change in flow rate. Since a base size smaller than 0.5 mm did not significantly change the results in any of the cylinder head configurations, this cell size was selected for each of them, and the simulation results were considered mesh independent. The italic cell counts in Tables 4 and 5 denote the final simulations with the 0.5 mm base size.

The cell counts for the exhaust simulations were larger, as they required larger plenums. Larger plenums were required by the exhaust simulations in order to capture the details of the jets created by the exhaust flows exiting the ports to open air. More cells and larger plenums allowed the jets' flows to develop and be fully resolved by the CFD software. Too small of a plenum resulted in numerically unstable simulations which cause erratic results and failures. The plenum sizes were also determined by an iterative process, with the final plenum dimensions of 15D selected for the exhaust simulations, where D was the effective diameter of each exhaust port. This size was the smallest possible that concluded in stable simulations for both the rotary and poppet valves in the exhaust configuration.

Table 6 CFD prism layer settings

# of prism layers	7
Prism layer near wall thickness	0.01 mm
Prism layer total thickness	0.5 mm
Stretching function	Geometric progression

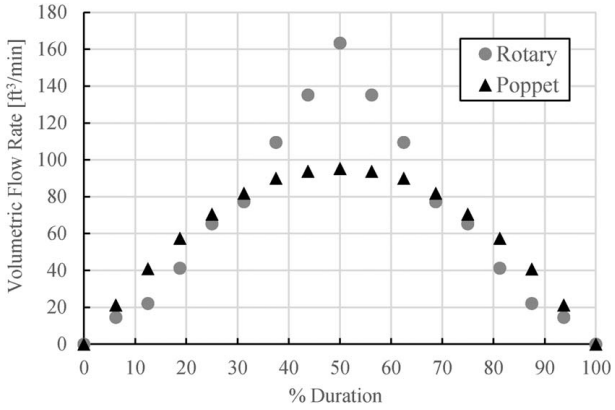

Fig. 10 Flow bench volumetric flow rate versus duration: intake configuration

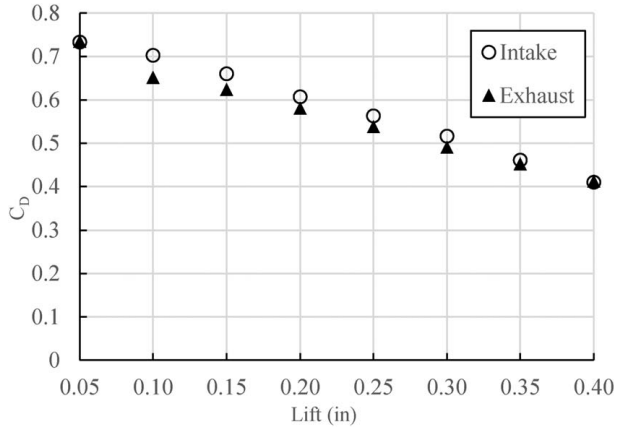

Fig. 12 Discharge coefficient versus lift for poppet valve head

The prism layer settings are shown in Table 6. These settings were designed to capture the boundary layer entirely and achieve $y+$ values of less than 1 in the near wall adjacent cells.

5.2 Boundary Conditions. Each simulation used plenums on both the intake and exhaust sides of the engine to allow flow development to occur outside of the actual inlet and outlet surfaces. In each configuration, the inlet face, depicted at the top left of each diagram in Fig. 9, was set as a stagnation inlet, with the specified 25 in. of water (6.221 kPa) inlet pressure. The outlet face, depicted as the bottom lines on the cylinder diagrams in Fig. 9, was set as a pressure outlet. The apparent discontinuity of the poppet valve mesh is due to the asymmetry of the poppet valve intake port. The inlet and outlet faces were on the outside of the plenums. The walls of the plenums were set to be frictionless since they were not actually present during flow bench testing and were created solely for the purpose of the simulations. The remaining initial conditions were defined to match the environmental conditions during the flow bench testing.

6 Results and Discussion

6.1 Flow Bench Results. The flow rate results from the steady-state flow bench study are shown in Figs. 10 and 11. Comparing the area under each flow curve reveals that the rotary valve has a higher total flow capacity than the poppet valve used in this study. In both the intake and exhaust configurations, the rotary valve head showed a lower flow rate on the lower end of valve opening but overcame the poppet valve after the 30% duration mark, increasing its flow advantage until full opening at 50% duration. The slight disadvantage of the rotary valve at low duration was made up for by the large flow advantage it exhibited at the top end of duration. It should be noted once again that the rotary valves used in this study are significantly undersized with respect to the poppet valves' curtain areas, which affects the low-opening flow rates. The graphical results from Figs. 10 and 11 can been seen in tabular form in Tables 4 and 5.

Figure 12 shows that the discharge coefficient of both intake and exhaust poppet valves decreased as the valve lift increased. Previous studies have shown behavior consistent with these results [8,9]. The values found for C_D of the poppet valves are also consistent with the range of values from the previous research.

The rotary valve discharge coefficient, as seen in Fig. 13, exhibited the opposite behavior. As the valve opened more, the C_D increased until it was near an optimal value of 1.0 at full opening. The exhaust valve showed a higher C_D value at every valve opening position on the rotary cylinder head as compared to the intake valve's performance. This is most likely a result of the differing port geometries between the two valves.

6.2 Computational Fluid Dynamics Results. The CFD testing was validated by the data collected during the flow bench testing. The only measured data point available was the volumetric flow rate, so the CFD data were compared to the flow bench test data for validation of the CFD methodology.

Tables 7 and 8 show the comparison between the results of the flow bench and CFD tests. Based on the measured error from the flow bench data, most of the CFD results were within the typical 5% margin of an analog flow bench manometer.

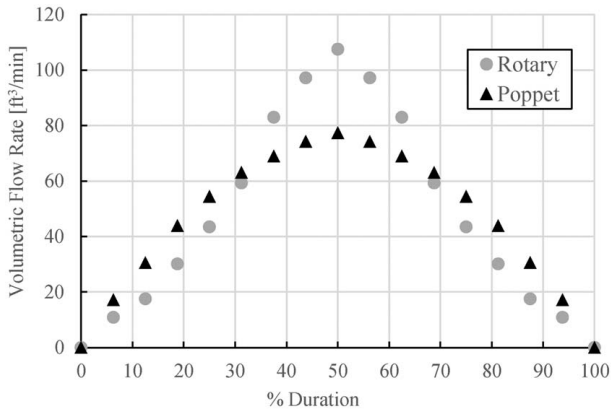

Fig. 11 Flow bench volumetric flow rate versus duration: exhaust configuration

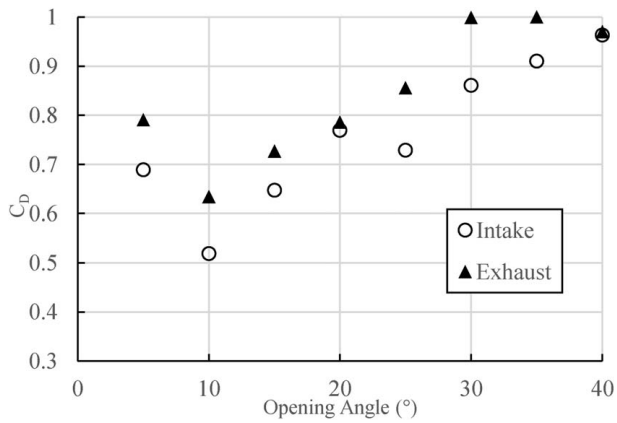

Fig. 13 Discharge coefficient versus valve angle for rotary valve head (40 deg is fully open)

Table 7 Comparison of flow bench and CFD volumetric flow rate data for the poppet valve cylinder head configuration

	Poppet intake ft^3/min (m^3/min)			Poppet exhaust ft^3/min (m^3/min)		
% Duration	Flow bench	CFD	% Diff.	Flow bench	CFD	% Diff.
5	21.3 [0.60]	20.9 [0.59]	−1.88	17.2 [0.49]	17.1 [0.48]	−0.86
10	40.8 [1.16]	41.3 [1.17]	1.16	30.6 [0.87]	30.4 [0.86]	−0.58
15	57.5 [1.63]	56.8 [1.61]	−1.23	43.9 [1.24]	44.2 [1.25]	0.67
20	70.5 [2.00]	70.9 [2.01]	0.57	54.5 [1.54]	55.1 [1.56]	1.12
25	81.8 [2.31]	84.4 [2.39]	3.24	63.1 [1.79]	64.3 [1.82]	1.88
30	90.0 [2.55]	92.4 [2.62]	2.67	69.0 [1.95]	71.0 [2.01]	2.91
35	93.8 [2.65]	94.2 [2.67]	0.48	74.3 [2.10]	74.5 [2.11]	0.32
40	95.3 [2.70]	96.1 [2.72]	0.89	77.4 [2.19]	76.7 [2.17]	−0.93

Table 8 Comparison of flow bench and CFD volumetric flow rate data for the rotary valve cylinder head configuration

	Rotary intake ft^3/min (m^3/min)			Rotary exhaust ft^3/min (m^3/min)		
% Duration	Flow bench	CFD	% Diff.	Flow bench	CFD	% Diff.
5	14.6 [0.41]	14.8 [0.42]	1.31	10.9 [0.31]	11.0 [0.31]	0.51
10	22.0 [0.62]	22.1 [0.63]	0.41	17.6 [0.50]	17.4 [0.49]	−0.87
15	41.2 [1.17]	42.1 [1.19]	2.23	30.2 [0.85]	30.6 [0.87]	1.38
20	65.3 [1.85]	66.2 [1.87]	1.46	43.5 [1.23]	44.0 [1.25]	1.12
25	77.3 [2.19]	77.5 [2.19]	0.32	59.3 [1.68]	59.7 [1.69]	0.76
30	109.5 [3.10]	109.9 [3.10]	0.37	83.0 [2.35]	82.6 [2.34]	−0.42
35	135.1 [3.83]	135.2 [3.83]	0.05	97.2 [2.75]	96.6 [2.74]	−0.59
40	163.4 [4.63]	163.8 [4.63]	0.28	107.4 [3.04]	102.3 [2.98]	−4.80

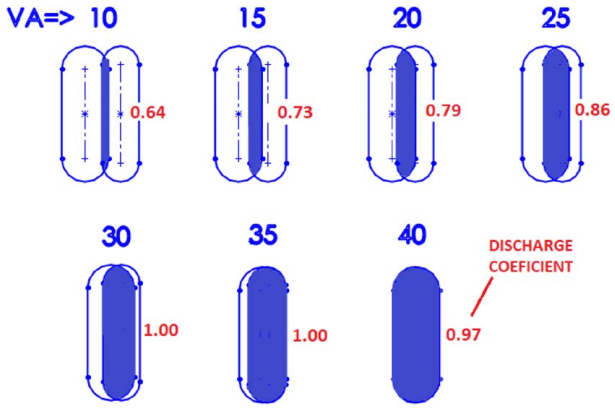

Fig. 14 Graphical representation of the open flow area of a rotary exhaust valve at discrete valve angle positions

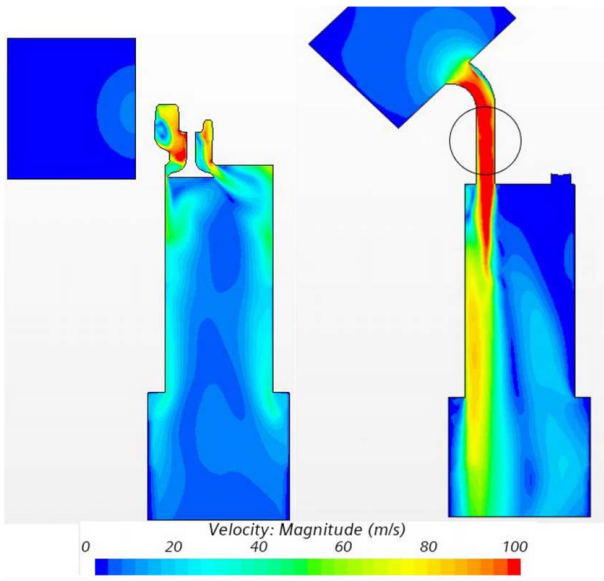

Fig. 15 Velocity magnitude at the cylinder center plane: intake configuration, valves fully open

Figure 14 graphically shows the various flow openings by degrees of crank angle for the rotary exhaust valve of the engine. The outlines are the openings in the rotary valve and cylinder head, and the solid regions are the area of overlap at each increment. It can be observed that, even at low-opening values, the rotary valve can produce high discharge coefficients due to the unobscured flow path. The coefficient at wide open (40 valve angle degrees) is less than unity as a result of the 5% error range of the measurement equipment. The intake valve of this exercise had a similar geometry and scale.

Velocity in any given port is desirable, as it correlates to higher mass flow rates for a given pressure drop. Figures 15 and 16 show the velocity profiles on a cut plane at the valve port centerline, comparing the poppet valve (left) to the rotary valve (right). At the fully open position, the rotary valve exhibits much higher velocity airflow throughout the valve ports in both intake and exhaust configuration. The unobstructed flow path of the rotary valve allows for the development of a flow jet, with most of the air in both ports flowing at a velocity at or above 100 m/s (328 fps). The poppet valve obstructs the flow, leading to generally lower velocities through the port.

In the fully open position, the flow in the rotary valve ports shows very little separation from the port walls outside of the small bend near the top of the cylinder head. The resulting lack of separation allows the flow to maintain its energy in the direction of the pressure gradient. The poppet valves show significant turbulence and flow separation within the ports. The geometry changes and the obstruction of the valve both contribute to the frictional losses of the flow, which results in decreased mass flow in both intake and exhaust configurations.

The rotary valves, even with smaller flow areas, exhibited higher mass flow rates than the poppet valves. The total area under the intake

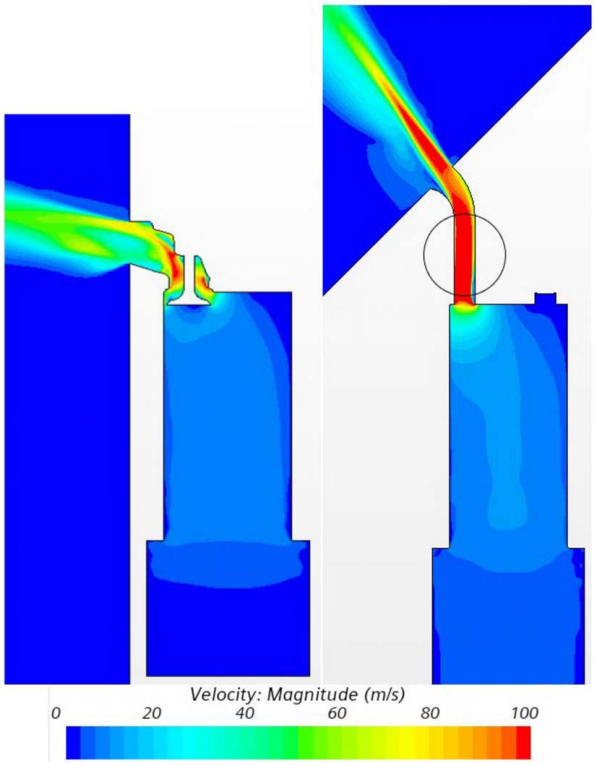

Fig. 16 Velocity magnitude at the cylinder center plane: exhaust configuration, valves fully open

flow curve is higher for the rotary valve, despite the poppet valve having 37.1% larger flow (curtain) area. For the exhaust rotary valve, the area under the flow curve is also of larger magnitude, even though the poppet exhaust valve has 69.4% more flow area. At small openings, the flow was more affected by the smaller port areas of the rotary valves. At larger openings, the higher discharge coefficients of the rotary valves provided more gas flow.

This difference in flow is due to the higher discharge coefficient of the rotary valve as compared to the poppet valve. At full opening, the discharge coefficients of the rotary valves were approximately 0.96–0.97 compared to values of around 0.40–0.41 for the poppet valves (intake and exhaust, respectively).

As mentioned above, the rotary valve port sizes chosen for this exercise were done so to match the minimum cylinder head port size of the standard poppet valve engine. In practice, the rotary valve ports' sizes could be enlarged to significantly increase the air flow of both the intake and exhaust without adding weight, cost, or undue packaging constraints (which is an issue for poppet valves) to optimize cylinder head gas exchange processes.

7 Summary/Conclusions

The data presented in this paper show that in steady-state, cold flow conditions, the rotary valve cylinder head outperforms a conventional poppet valve cylinder head when attached to the same engine. The total mass flow across the opening range for the rotary valve was higher despite it having a lower cross-sectional area for both the intake and exhaust valves. At full valve opening, the rotary valve outflowed the poppet valve by 23% in exhaust and 52% in intake. While the port sizes used for this research were equal for comparison, the rotary valve ports could be sized larger without issue. An increased port size would increase the flow capabilities of the rotary valve head even further without the packaging constraints of a typical poppet valvetrain.

The increased flow capacity of the rotary valve correlates with a higher volumetric efficiency. Higher volumetric efficiency is generally associated with improved specific power output and lower specific fuel consumption in an IC engine.

8 Future Work

Potential future work on this topic includes additional full-scale dynamometer testing of working engines with both rotary and poppet valve designs on the same base engine. This would be used to explore items such as optimized valve timing and potential increases in compression ratio. Additionally, further research into the endurance characteristics of this rotary valve design is needed.

Future CFD work could include transient, unsteady simulations as well as those with full engine motion, providing a full picture of the dynamic performance of the rotary valve beyond the incremental steady-state data captured for this paper. The addition of tumble and swirl measurement to the flow bench could add value to the CFD comparison, but such equipment was unavailable at the time of this study.

Acknowledgment

Special thanks to everyone at UNCC and Vaztec who helped with this project along the way.

Conflict of Interest

There are no conflicts of interest. This article does not include research in which human participants were involved. Informed consent not applicable. This article does not include any research in which animal participants were involved.

Data Availability Statement

The datasets generated and supporting the findings of this article are obtainable from the corresponding author upon reasonable request.

References

[1] Mason, B., and Lawes, K., 2014, "Rotary Valve Four-Stroke Technology Applied to Handheld Power Tools," SAE Technical Paper 2014-32-0111.
[2] Boretti, A., and Scalzo, J., 2015, "Turbo/Supercharged Two/Four Stroke Engines With One Intake and One Exhaust Horizontal Rotary Valve Per Cylinder and Central Direct Injection and Ignition," SAE Technical Paper 2015-26-0031.
[3] Muroki, T., Moriyoshi, Y., and Sekizuka, S., 1999, "A Study of Rotary Valve for a Single Cylinder Engine," SAE Technical Paper 1999-01-3322.
[4] Hunter, 1946, *Rotary Valve Engines*, John Wiley Publishing, New York, pp. 32–47.
[5] Vaseleniuck, 2015, "Head Assembly For an Internal Combustion Engine," US Patent 9,115,606.
[6] Palmisano, R., and Ng, H. D., 2012, "Design Analysis and Comparison Between Standard and Rotary Porting Systems for IC Engine," Int. J. Autom. Technol., **13**(2), pp. 175–791.
[7] Blair, G. P., Lau, H. B., Cartwright, A., Raghunathan, B. D., and Mackey, D. O., 1995, "Coefficients of Discharge at the Apertures of Engines," SAE Technical Paper 952138.
[8] Zirngibl, S., Held, S., Prager, M., and Wachtmeister, G., 2017, "Experimental and Simulative Approaches for the Determination of Discharge Coefficients for Inlet and Exhaust Valves and Ports in Internal Combustion Engines," SAE Technical Paper 2017-01-5022.
[9] Heywood, J. B., 1988, *Internal Combustion Engines Fundamentals*, McGraw-Hill, New York.
[10] Shih, T.-H., Liou, W. W., Shabbir, A., Yang, Z., and Zhu, J., 1995, "A New k–ε Eddy Viscosity Model for High Reynolds Number Turbulent Flows," Comput. Fluids, **24**(3), pp. 227–238.
[11] Menter, F. R., 1994, "Two-Equation Eddy-Viscosity Turbulence Models for Engineering Applications," AIAA J., **21**(11), pp. 1525–1532.
[12] Abe, K., Kondoh, T., and Nagano, Y., 1994, "A New Turbulence Model for Predicting Fluid Flow and Heat Transfer in Separating and Reattaching Flows," Int. J. Heat Mass Transfer, **37**(1), pp. 139–151.
[13] Manceau, R., and Hanjalic, K., 2002, "Elliptic Blending Model: A New Near-Wall Reynolds-Stress Turbulence Closure," Phys. Fluids, **14**(2), p. 744–754.
[14] Durbin, P. A., 1996, "On the k–e Stagnation Point Anomaly," Int. J. Heat Mass Transfer, **17**(1), pp. 89–90.